Locally self-similar, finite-time collapse in a high-symmetry vortex filament model

R. B. Pelz*
Mechanical and Aerospace Engineering, Rutgers University, Piscataway, New Jersey 08855-0909
(Received 14 May 1996; revised manuscript received 10 October 1996)

A locally self-similar solution is found using a vortex filament model. The solution is steady in a rescaled frame with magnification $(t_{\rm crit}-t)^{-1/2}$ about the origin. A finite-time singularity results in which velocity, vorticity, and enstrophy scale as $t_{\rm crit}-t$ to powers $-1/2$, -1, and $-1/2$, respectively. The initial flow is six closed vortex contours symmetric around and propagating toward the origin. The self-similar inner solution consists of three orthogonal filament quadrupoles centered about the origin. The solution is attracting within a space of symmetries preserved by the incompressible Navier-Stokes and Euler equations. The numerical method consists of piecewise straight vortex segments with a standard variable core regularization model. Small core deformation is modeled with a two-length scale core function. This solution is similar to the candidate singular flow suggested by Boratav and Pelz [Phys. Fluids **6**, 2757 (1994)] in their large-scale pseudospectral simulations. The steady inner solution has a set of hyperbolic critical points around which singular focusing occurs. It is conjectured that the singularity is pointwise in time as well as in space, and a smooth expanding solution exists which is symmetric with the collapsing solution about the critical time. [S1063-651X(97)15202-3]

PACS number(s): 47.15.Ki, 03.40.Gc, 47.32.Cc

I. INTRODUCTION

The assumption that smooth solutions to the equations of a three-dimensional incompressible flow exist for all time has not been proven. If a smooth initial flow were found that develops a singularity in finite time, the validity of the equations of ideal hydrodynamics would have to be reassessed. Such a flow, if stable, may also have applications such as focusing or rapid mixing. Many investigations, both analytic and numerical, have established bounds, conditions and possible candidate flows for a finite-time singularity (FTS), but none has shown its existence definitively [1].

Numerical solutions of Kerr [2] and Boratav and Pelz [3] present strong evidence of a FTS. Figure 1, from simulations in the latter reference, shows isosurfaces of vorticity magnitude (a) at an early time and low magnitude, and (b) at a late time and higher magnitude. The flow structure is termed a vortex dodecapole. The former isosurface is on the scale of the domain, and the latter on the scale of the grid size. The flow is highly symmetric, using all the symmetries of the Navier-Stokes equation, and appears visually self-similar. These simulations use a pseudospectral method with effective resolution of 1024^3 modes; one decade of $(t_{\rm crit}-t)^{-1}$ scaling in vorticity is found.

It is evident from this example that, with large-scale simulation, singular flows can only be suggested. The role of such simulations is to motivate possible analyses or simpler models which bring us closer to the establishment of a FTS.

In the present paper, a vortex filament method is used to model the collapsing vortex structure observed by Boratav and Pelz [3]. With a simpler model, higher resolution and a better understanding of the solutions can be achieved. In Fig. 1, the vortex lines are approximately tangent to the surface, but intersect it at the ends. The topology of the tubes is rather simple. The radius of curvature of the tubes appears to be large compared to the core thickness. The isosurface of vorticity actually appears more cylindrical at later times, suggesting that core deformation is slight. For these reasons, we believe that this flow can be modeled with a filament method.

We show in this paper that there exists a steady collapsing solution to a vortex filament model of the vortex dodecapole shown in Fig. 1. The steady solution is in a frame rescaled about the origin such that the magnification is $(t_{\rm crit}-t)^{-1/2}$. Since the spatial scale goes to zero in finite time, the induced velocity scales as the magnification. Since the core size goes to zero, constant circulation causes the vorticity to scale as $(t_{\rm crit}-t)^{-1}$. The same inner solution was found for different initial positions and core thicknesses. Thus a finite-time singularity is found in the filament model in the form of an attracting, locally self-similar collapsing solution.

In a series of papers, Siggia and Pumir presented evidence of a FTS in which two vortex filaments align in an antiparallel fashion and collapse. Initially they found that the ratio

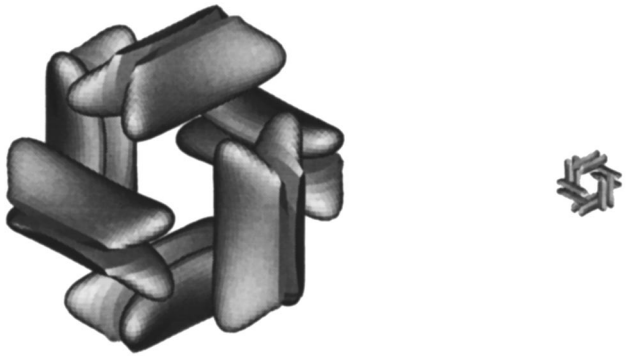

FIG. 1. Isosurfaces of vorticity magnitude from large-scale simulations: (a) at $t=1.5$ and $|\omega|=10$, and (b) at $t=2.125$ and $|\omega|=100$.

*FAX: 908-445-3653, -5313. Electronic address: pelz@jove.rutgers.edu

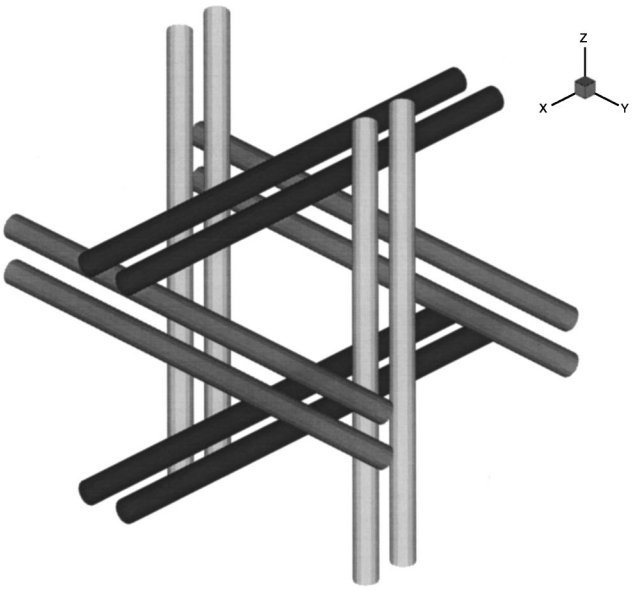

FIG. 2. The straight-line filament dodecapole.

of radius of curvature to core size approached unity, making the filament approximation an invalid model of the Euler equations [4,5]. Later, they showed, with a locally conservative core model, that the ratio does remain greater than 1, but the cores overlap significantly [6]. Waele and Aarts [7] also studied the antiparallel collapse problem with a filament model. They showed evidence of a FTS up to the point when the cores overlapped. Finally, Pumir and Siggia showed that core deformation in a Eulerian simulation (which would occur at the time of filament core overlap) caused a saturation of the axial strain rate which allowed only an exponential blow-up [8]. This finding was substantiated by simulations of Shelley, Meiron, and Orszag [9]. In the simulations of Kerr [2], singular behavior was observed for the antiparallel collapse problem if the initial flow was carefully filtered.

The filament solution presented in this paper does not involve an antiparallel collapse. The solution does involve six vortex dipoles, but their position from the origin, separation distance and core radius all scale as $\sqrt{t_{\rm crit}-t}$. At the critical time, all 12 vortices have converged to the origin, and the core radius there has shrunk to zero.

Mild core deformation seen in the field simulations is modeled in our filament computation by a two-length-scale desingularization. With this, there is no core overlap of nonlocal vortex segments. While we find no evidence in the field or filament simulations of strong strain rates which would cause large core deformation in the field solution, this effect is not accounted for in the filament model. If present in the field solution, core deformation dynamics could cause a major difference between the field and filament solutions.

Physically, in order for a FTS to occur through vortex stretching, the rate of strain along the axis of the vortex should increase with the vorticity. In the vorticity isosurface plot of the dodecapole in Fig. 1 or its filament conceptualization, Fig. 2, such a connection can be seen. Each quadrupole creates a strain field along the axis of the quadrupole which lies orthogonally inside it. The vortex tubes are stretched and the vorticity is increased. As the two dipole pairs of each quadrupole advect toward the origin, the axial strain rate they exert on the inside quadrupole also increases. This flow may exhibit the necessary feedback mechanism between vorticity and axial strain rate.

The organization of the paper is as follows. In Sec. II we present the vortex filament model with piecewise linear segments and variable core function. We then describe, in Sec. III, the dynamic rescaling technique employed in the Lagrangian frame. In Sec. IV we briefly describe how the initial condition for the filaments was constructed. The results of the computations are presented in Sec. V. A modification of the filament model which takes into account local core deformation is then discussed in Sec. VI. The solution after the critical time is discussed in Sec. VII, and concluding remarks are made in Sec. VIII.

II. VORTEX FILAMENT MODEL

To construct a vortex filament model of the dodecapole shown in Fig. 1, we make the following assumptions and restrictions.

(i) Each of the vortex tubes seen in Fig. 1 can be replaced by single vortex filament. It is observed that the cores remain separate and do not interact significantly, the core thickness is on the order of the distance to the closest bilateral symmetry plane, and the radius of curvature is greater than the core thickness. An isolated and concentrated vorticity distribution is necessary for the filament model to approximate the Euler equations.

(ii) Bilateral symmetry on all the ''0'' planes, which is preserved by the Navier-Stokes equations, is used. From this symmetry, the streamlines lie in the ''0'' planes and on the axes. The axes are vorticity nulls, and only normal vorticity may be nonzero on the planes. The tangential vorticity near the plane has an equal and opposite image vorticity across the plane.

(iii) The permutation symmetry on vorticity, $\omega_x(x,y,z)=\omega_y(z,x,y)=\omega_z(y,z,x)$, which is also preserved by the equations of motion, is used. This symmetry is important because it allows a coupling between the vorticity of a tube and the externally applied axial strain rate. It was not used in the high-symmetry Taylor-Green vortex simulations of Brachet *et al.* [10], which yielded only exponential growth.

The stability of the solutions to symmetry-breaking perturbations will not be addressed here. Our approach is to gather evidence for the existence of a FTS in a restricted space first. While we do not speculate on stability, the establishment of even an unstable solution trajectory, which ends in a FTS, is important.

We consider a filament beginning in the plane $z=0$ close to the origin with the vector pointing into the first octant $(x,y,z>0)$. The filament extends orthogonally into the first octant, and ends in the plane $x=0$ (again orthogonally) further away from the origin. (We shall also consider a filament which ends in the plane $y=0$.) This fundamental filament is a smooth space curve represented by $\vec{x}(s)$, where s is the arc length from 0 at the $z=0$ plane to s^* at the $x=0$ plane. The bilateral symmetries create, from the fundamental filament, a closed contour lying in the $y>0$ half-space and an image contour in the $y<0$ half-space. From the permutation symmetry, an image of the fundamental filament, extending from

the $x=0$ plane, plus the bilateral images, make up two contours. Another application of the permutation symmetry gives two more. Thus six closed filament contours are created which are completely determined by the fundamental.

The fundamental vortex filament curve $\vec{x}(s)$, $s=[0,s_*]$ is discretized for numerical computation into N piecewise straight vortex segments connected end to end, the ith extending from $\vec{x}_{i-1}$ to $\vec{x}_i$, $i=1,2,\ldots,N$. $\vec{x}_0=\vec{x}(0)$ $\vec{x}_N=\vec{x}(s_*)$. The velocity field at point $\vec{x}$, induced by a straight vortex filament with end points 1 and 2, is

$$\vec{u}_{1,2}(\vec{x})=\frac{\Gamma}{4\pi}\left(\frac{\vec{x}-\vec{x}_1}{|\vec{x}-\vec{x}_1|}-\frac{\vec{x}-\vec{x}_2}{|\vec{x}-\vec{x}_2|}\right)\cdot(\vec{x}_2-\vec{x}_1)\frac{(\vec{x}-\vec{x}_1)\times(\vec{x}-\vec{x}_2)}{|(\vec{x}-\vec{x}_1)\times(\vec{x}-\vec{x}_2)|^2},\tag{2.1}$$

where Γ is the circulation. A core-cutoff function is used to avoid the singularity inherent in an infinitesimally thin filament with nonzero curvature. We use a cubic Gaussian core function for the vorticity distribution (see Knio and Ghoniem [11], Leonard [12], and Fernandez, Zabusky, and Gryanik [13] for more details). A local, volume-conserving expression is used to update the core thickness σ for each segment: $\sigma_i^2|\vec{x}_{i+1}-\vec{x}_i|=\text{const}$. The velocity at a point on the fundamental filament has a contribution from all the other segments of the fundamental plus all the segments on the 23 image filaments obtained by applying the symmetries. The system is closed upon evaluation of the velocity at each segment end point of the fundamental filament, as

$$\vec{u}(\vec{x}_i)=\sum_{j=1}^{24N}\vec{u}_{j-1,j}(\vec{x}_i)\left[1-\exp\left(-\left(\frac{r_{i,j}}{\sigma_{i,j}}\right)^3\right)\right],\quad i=0,1,\ldots,N,\tag{2.2}$$

where $r_{i,j}=|\vec{x}_i-(\vec{x}_{j-1}+\vec{x}_j)/2|$ and $\sigma_{i,j}=\sqrt{\sigma_i^2+[(\sigma_{j-1}+\sigma_j)/2]^2}$. The circulation has been set to 4π. The endpoints are advected using a second-order Runge-Kutta scheme. A variable time step is set as a function of maximum rate of strain.

In the interaction region the filaments experience a large axial strain rate, so a remeshing algorithm is employed as needed to keep segment lengths approximately one-quarter (or one-eighth) of the smallest length scale. Cubic splines are used to construct interpolating polynomials for $x(s)$, $y(s)$, $z(s)$, and $\sigma(s)$ from the current distribution of segment end points. A more regular distribution for the segment end points is then found. Both equal-length segments throughout the contour and segments which are equal in the near field and stretched in the far field were used, with similar results.

A modification to the spherically symmetric core function into a two-length desingularization was introduced to model the slight core deformation encountered in the solution. It will be described in more detail in Sec. VI and in Pelz [14].

III. DYNAMIC RESCALING

A self-similar FTS can be found through the establishment of a transformation or rescaling of the Euler equations in which the solution is locally steady. In this section, we present such a scaling and apply it to the filament model.

We define a transformed spatial variable $\vec{\xi}$, in which the minimum interfilament distance is order unity. Since the collapse of the vortex filament is expected to be isotropic and about the origin, the transformation is $\vec{\xi}=S(t)\vec{x}$, where the scaling metric S is a function of time only. In keeping with the initial condition of $x_0(t=0)=1$, the scaling metric was chosen to be

$$S(t)=\frac{1}{x_0(t)}\tag{3.1}$$

so as to keep $\vec{\xi}_0(t)\cdot\hat{i}$ unity.

The velocity $\vec{v}$ in the rescaled plane is easily seen to be $\vec{v}=\vec{u}/S$, and is also of unit order. In this model, if the filaments collapse to the origin in real time [i.e., $1/S(t_{\text{crit}})=0$], the induced velocity on the filaments at the origin is singular. Velocity derivative terms scale as S^{-2} in the rescaled plane. A rescaled time variable, τ, defined through the velocity derivative scale, is $d\tau=S^2dt$.

The equations of ideal hydrodynamics in a Eulerian frame are

$$\frac{\partial\vec{u}}{\partial t}+\vec{u}\cdot\vec{\nabla}\vec{u}=-\vec{\nabla}P,\quad \vec{\nabla}\cdot\vec{u}=0.\tag{3.2}$$

Using the transformed variables as defined above, the equations become

$$\frac{\partial\vec{v}}{\partial\tau}+(a(\tau)+\vec{v}\cdot\vec{\nabla}_\xi)\vec{v}=-\vec{\nabla}_\xi Q,\quad \vec{\nabla}_\xi\cdot\vec{v}=0,\tag{3.3}$$

where

$$a(\tau)=\frac{1}{S^3}\frac{dS}{dt}=\frac{d}{d\tau}\ln S,\tag{3.4}$$

and $\vec{\nabla}_\xi$ is the gradient with respect to ξ.

This scaling is equivalent to the method of dynamic rescaling used for the nonlinear Schödinger equations [15–17]. Their function $l(t)$ is the inverse of our $S(t)$. $S(t)$ must be chosen such that as $t\to t_{\text{crit}}$, v remains smooth, and $S(t)\to\infty$ fast enough so that $\tau\to\infty$.

If S were to have the form $(t_{\text{crit}}-t)^{-\alpha}$, then the function a in Eq. (3.4) would be a nonzero real value for $\alpha=\frac{1}{2}$ only. Furthermore, if a solution were to be self-similar with this scaling, it would manifest itself as a steady solution in the transformed plane. Now if a self-similar solution were found with $\alpha=\frac{1}{2}$ (as will be observed in the results of Section V), then $a\vec{v}$ would equal the solenoidal projection of $-\vec{v}\cdot\vec{\nabla}_\xi\vec{v}$. Using rotation form, we see that $a=-\vec{v}\cdot\vec{\nabla}\Pi/v^2$, where Π is the pressure head.

The vorticity equation in the transformed plane is

$$\frac{D\vec{\zeta}}{D\tau}+2a\vec{\zeta}=\vec{\zeta}\cdot\vec{\nabla}_x\vec{v}\tag{3.5}$$

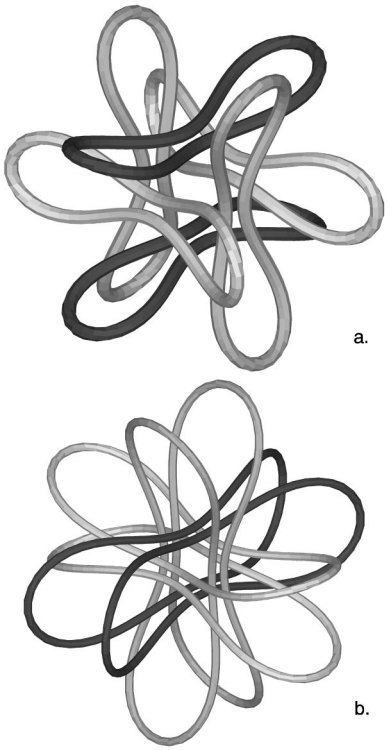

FIG. 3. Initial position of the vortex filament contours: (a) unlinked and (b) double Borromean Brunnian-linked hexaelastibons.

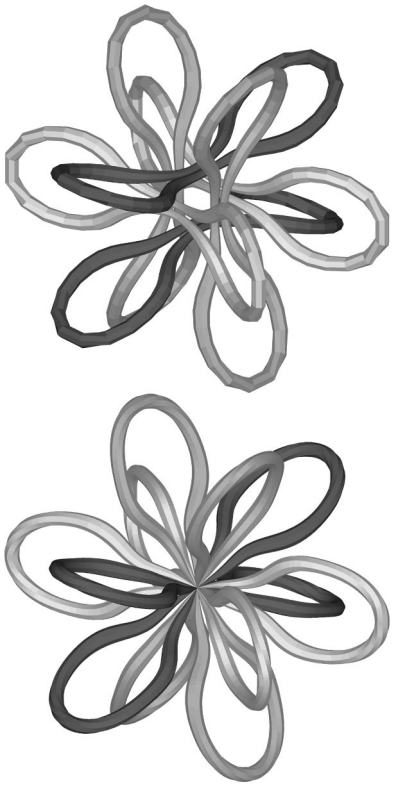

FIG. 4. Orthogonal view of the position of the filaments at 2 times during the evolution. The radius of the tubes is $\sigma/2$. The black, gray, and light gray tubes represent the three orthogonal filament loop pairs. The observer is at a fixed position with respect to the origin. The parameters for the top figure are $t=2.40$, $t_{\rm crit}-t=0.805$, and $S=2.14$, and the number of segments is 50. The parameters for the bottom figure are $t=3.20$, $t_{\rm crit}-t=0.967\times10^{-5}$, and $S=599$, and the number of segments is 242.

where $\vec{\zeta}=\vec{\omega}S^{-2}$. For the self-similar case, a is then half the strain rate along the axis of the vortex filament.

The equation for the advection of passive tracers in the rescaled plane is

$$\frac{D\vec{\xi}}{D\tau}=a\vec{\xi}+\vec{v}. \tag{3.6}$$

There is a nonsolenoidal source flow from the origin.

IV. INITIAL CONDITION

To solve the initial value problem given in Eqs. (2.1) and (2.2), we must construct a reasonable initial configuration for the filament contours. The initial condition of the vortex filament should form a closed contour in $\mathbb{R}^3$, be close to the straight line dodecapole in the vicinity of the origin, and have an outer region with minimal curvature. This last condition allows the time scales in the outer part of the filament to be greater than those of the inner part.

A smooth closed space curve that fits the conditions above can be found through the equations of an elastica. The development of the general problem can be found in Bottega [18]; we include only a brief description here.

To form a contour, a straight elastic rod is bent into a circle. The two ends are then ''taped'' together and an inward force is applied on either side of the ring to deform it into a dumbbell shape. Another force is applied at the tips in the binormal direction to give the rod out-of-plane curvature.

We shall consider unlinked and Brunnian-linked (double Borromean) combinations of the six rods. (Brunnian describes a link in which the removal of one component gives the unlink.) The unlinked configuration is as follows. A bent elastic rod is centered on the y axis with the semimajor and semiminor axes in the z and x directions, respectively. The closest distance to the origin is in the $z=0$ plane at the point $(1,r,0)$. The arclength of the rod is set such that the point of zero curvature is at $z=r$. An image is created by reflection about the $y=0$ plane and four more images are created through the permutation symmetry.

The double Borromean link is created by centering a rod on the $x=0$ axis. Semimajor and semiminor axes are in the z and y directions. The closest point to the origin is in the $z=0$ plane at $(1,r,0)$. The resulting ''hexaelastibons'' are shown in Fig. 3: (a) unlinked and (b) Brunnian linked. The three pairs of contours are colored black, dark gray, and light gray.

V. RESULTS

The initial value problem for the motion of the vortex filaments is solved numerically, and the results are presented in this section. The major finding is that in the rescaled $\vec{\xi}$ coordinates, one locally steady solution is found from numerous initial configurations. We first display the position of the vortex filament for a visual demonstration of local self-similarity. More quantitative results are then presented on scaling and the behavior of the velocity and pressure in the collapse region. A set of hyperbolic critical points within the

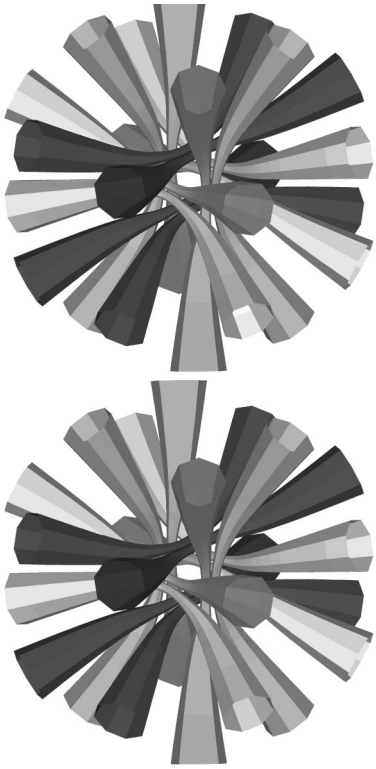

FIG. 5. Orthogonal view of the position of the filaments at two times during the evolution. The observer is at a fixed position with respect to the origin in the rescaled frame. Only the inner portion of the filaments are shown. The parameters for the top figure are. $t_{\rm crit}-t=0.200\times10^{-3}$ and $S=132$, and the number of segments is 134. The parameters for the bottom figure are $t_{\rm crit}-t=0.305\times10^{-7}$ and $S=10\,640$, and the number of segments is 890.

collapse region is examined, and the evolution of a material surface is followed to illustrate the potential of this solution for singular focusing. All computations were performed on a workstation with multidecade scaling firmly established in runs with a duration of no longer than a day.

Figure 4 shows the position and thickness of the filaments

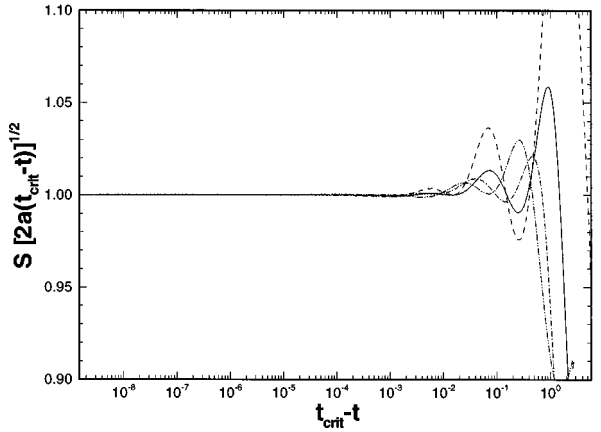

FIG. 6. The scaling metric S, multiplied by $[2a(t_{\rm crit}-t)]^{1/2}$ vs $t_{\rm crit}-t$. The unlinked initial condition with $\vec{x}_0=(1,4.45,0)$ is shown with a solid line, (1,7.48,0) dashed, (1,3.64,0) dot-dashed, and a linked initial condition (1,4,0) dot-dot dashed.

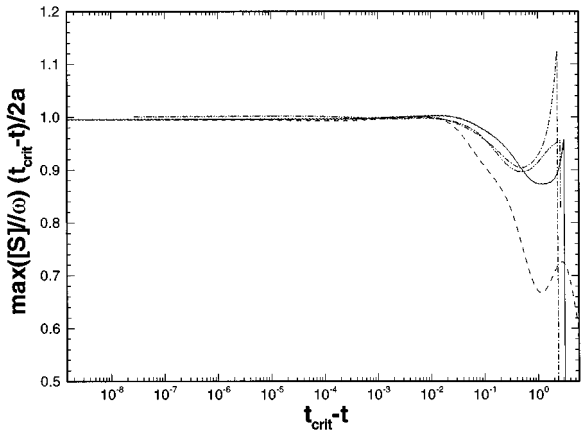

FIG. 7. The maximum axial strain rate multiplied by $(t_{\rm crit}-t)/2a$ vs $t_{\rm crit}-t$ for the same cases as in the previous figure. The maximum occurs at $\vec{x}_0$.

at two times in the evolution. The thickness shown is half of the core radius; no eccentricity is shown. The top view is at a time 2.40 ($t_{\rm crit}-t=0.805$). The scaling metric S is 2.14, which means that x_0 has decreased from 1 initially to 0.467. The bottom view is at a later time of 3.20 ($t_{\rm crit}-t=0.967\times10^{-5}$). The metric is 599, so x_0 is 0.167×10^{-2}. From this stationary view, the tubes in the bottom view appear to eminate radially from the origin. The outer part of the loop moves only slightly during this time.

Figure 5 again shows the position and thickness at two (different) times in the evolution. The observer is at a constant distance from the origin in the rescaled frame, and only the region around the origin is shown. The structure of the three orthogonal quadrupoles, or dodecapole, is clearly seen. The top view is at a time $t_{\rm crit}-t=0.210\times10^{-3}$, and has a scaling metric of 132. The bottom view is at a later time of $t_{\rm crit}-t=0.31\times10^{-7}$, and has a metric of 10 640. While the collapse toward the origin is apparent in Fig. 4, the two views in Fig. 5 look identical, despite the difference in magnification of a factor of 100. This is the structure of the self-similar solution.

Figure 6 shows a plot of the scaling metric, S, multiplied by $\sqrt{2a(t_{\rm crit}-t)}$ versus $(t_{\rm crit}-t)$. A number of runs are

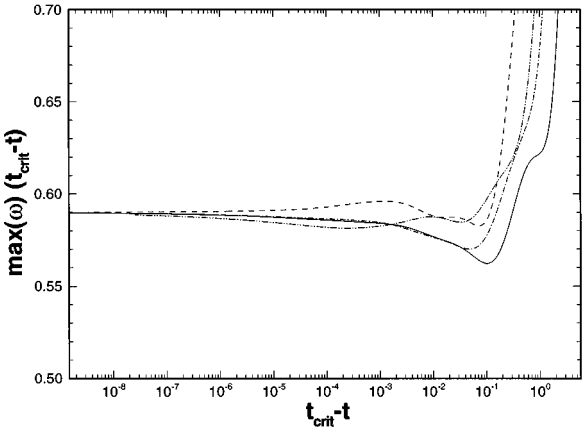

FIG. 8. The maximum of the vorticity multiplied by $t_{\rm crit}-t$ vs $t_{\rm crit}-t$.

shown, including the unlinked initial condition with $\vec{x}_0=(1,4.45,0)$ (solid), (1,7.48,0) (dashed), (1,3.64,0) (dot-dashed), and a linked initial condition (dot-dot dashed). For all initial conditions, the function $a(t)$ converged to a value of 0.144 . . . . The critical time, which was calculated by extrapolating $1/S$ to zero, is a function of the initial condition. Within about four orders of magnitude decrease in $(t_{\rm crit}-t)$, the transients have decayed to reveal the self-similar solution.

Figure 7 shows a plot of the maximum axial strain rate on the filament (which occurs in the $z=0$ plane of the fundamental filament) multiplied by $(t_{\rm crit}-t)/2a$ versus $(t_{\rm crit}-t)$. A similar scaling is found for the maximum vorticity, as shown in Fig. 8. Scaling for these quantities can be inferred from the behavior of S, but is shown to illustrate the $(t_{\rm crit}-t)^{-1}$ scaling of the sup norm of velocity derivatives in agreement with the theorems of Ponce [19] and Beale, Kato, and Majda [20]. The transients in the vorticity are longer lived due to the rather slow convergence of the core thickness to its asymptotic value.

Figure 9 shows a plot of the enstrophy multiplied by $\sqrt{t_{\rm crit}-t}$ versus $t_{\rm crit}-t$. The reason for the $(t_{\rm crit}-t)^{-1/2}$ scaling is as follows. The enstrophy is proportional to the integral along the filament of the inverse of the core cross-sectional area. The integrand scales as $(t_{\rm crit}-t)^{-1}$ along the inner length, which scales as $\sqrt{t_{\rm crit}-t}$. The contribution from the complement of the filament is negligible after some time. Multiplying the integrand scaling by the length over which the scaling acts gives the desired result.

Figure 10 shows a plot of the arc length of the fundamental filament normalized by its initial value versus $t_{\rm crit}-t$. The arc length does not scale with $t_{\rm crit}-t$. This can be seen from the perspective views of the evolution in Fig. 4. The arc length of the inner region scales as $\sqrt{t_{\rm crit}-t}$, leaving the slowly changing arc length in the outer region to dominate.

In the rescaled plane, the velocity field is composed of the induced velocity from the filaments and the source flow $a\vec{\xi}$ [see Eq. (3.6)]. Along an axis, a positive source flow near the origin is met by a negative flow from the dipolar jet, creating a stagnation point. These six type-B hyperbolic critical points (one stable and two unstable manifolds) then move toward the origin as $\sqrt{t_{\rm crit}-t}$ in the $\vec{x}$ plane, and the eigenvalues scale as $(t_{\rm crit}-t)^{-1}$. A singular concentration of passive tracers and a stretching of passive vectors will occur at these points.

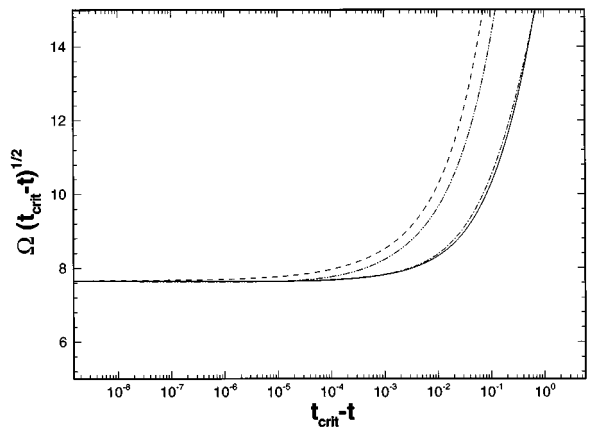

FIG. 9. The enstrophy multiplied by $(t_{\rm crit}-t)^{1/2}$ vs $t_{\rm crit}-t$.

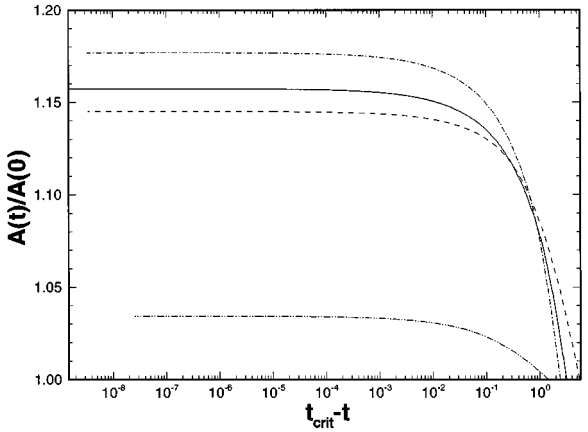

FIG. 10. The arc length of the fundamental filament vs $t_{\rm crit}-t$. The arc length is normalized by the value at $t=0$.

Since the local solution in the rescaled frame is steady, we can take the position of the filaments and the value of $a(\tau)$ at a late time as fixed, and examine the advection of fluid particles with Eq. (3.6). Fluid particles are initially placed as a mesh on one face of a cube centered at the origin, and with a side length of 8. Figure 11 shows the mesh surface at four different times in the evolution in the rescaled frame. The other faces are found through symmetries. The surface in the upper left is at a time $t_{\rm crit}/4$ after the initial time. The strain rate has increased by a factor of 1.3. The surfaces in the upper right, lower left, and lower right are at times $0.44t_{\rm crit}$, $0.58t_{\rm crit}$, and $0.68t_{\rm crit}$, with strain rate factors 1.8, 2.4, and 3.2. In the rescaled frame, the divergence is $3a$, so the volume of the cube is increasing. In the middle of each face, however, the particles near the critical points move very slowly. The large strain rate near these points can be seen from the curling and stretching of the faces.

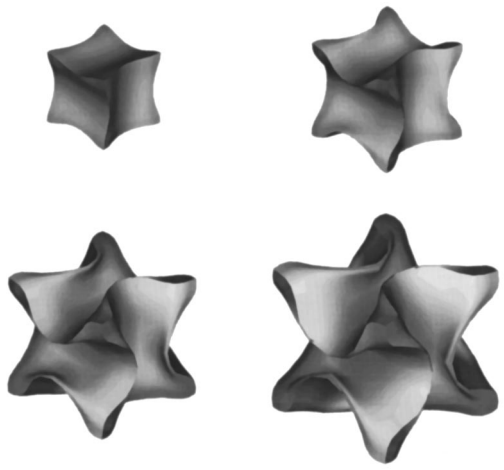

FIG. 11. Material surfaces advected by the flow as viewed in the rescaled frame. The surface is initially a cube with length 8. The top left, top right, bottom left, and bottom right are at times 0.25, 0.44, 0.58, and 0.68 times $t_{\rm crit}$ which are equal intervals in τ. Strain rate increases exponentially as $e^{2a\tau}$, with factors being 1.3, 1.8, 2.4, and 3.2 at the four times. The flattened areas, which are near the critical points, move only slightly.

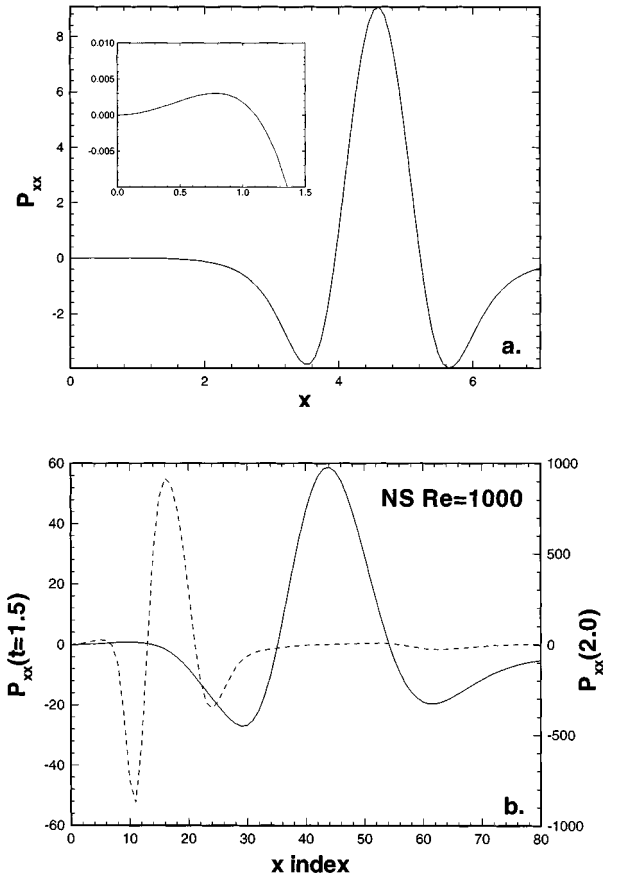

FIG. 12. $Q_{\xi\xi}$ is plotted along the ξ axis in (a) for the filament model ($S=10\,640$). The inset is a closeup of $Q_{\xi\xi}$ near the origin showing the lip of positive curvature. P_{xx} is plotted along the x axis in (b), the Navier-Stokes Eulerian simulations at times $t=1.5$ (left axis, solid) and $t=2.0$ (right axis, dashed).

Ng and Bhattacharjee [21] developed a sufficient condition for a FTS in symmetric flows. The condition that the fourth derivative of pressure at the origin be positive has a simple interpretation in the case of the self-similar solution. Letting ξ be one component of $\vec{\xi}$, and u be the velocity component in that direction, the pressure gradient along the axis can be written

$$\frac{\partial Q}{\partial \xi} = -\left(\frac{\partial u}{\partial \xi} + a\right) u, \tag{5.1}$$

since the axis is a streamline and the flow is steady near the origin. From incompressibility and symmetry, $u=-C\xi^3$ near the origin (and is valid to $\xi \approx 2$), where C is a positive constant. The fourth derivative of rescaled pressure at the origin is then

$$\frac{\partial^4 Q}{\partial \xi^4} = 6aC > 0. \tag{5.2}$$

Also, based on our scaling, $\partial^4 P/\partial x^4$ should scale as $(t_{\text{crit}}-t)^{-3}$.

Figure 12(a) shows $Q_{\xi\xi}$ along the ξ axis from the filament model, and Fig. 12(b) shows P_{xx} along the x axis for $t=1.5$ and 2 from the large-scale simulations of the Navier-Stokes equations [22]. There is a general agreement between the model and simulations. The ''negative-positive-negative'' behavior of the dipole is more concentrated in the model. Also, the asymmetry between the negative values is not seen in the model. The ''lip'' of slightly positive curvature near the origin, which makes P_{xxxx} positive at the origin, exists in the model also, as shown in the inset, but to a lesser magnitude.

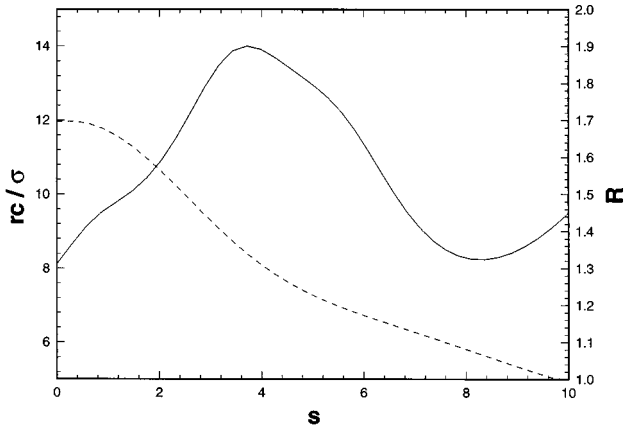

FIG. 13. The ratio of radius of curvature to core thickness vs arc length (solid line, plotted on left axis). The ratio of semimajor to semiminor length for the elliptical core model (dashed line, plotted on right axis).

For solutions of the filament model to represent those of the Euler equations accurately, the radius of curvature of the filament must be much larger than the core size at each point. In Fig. 13, we plot with a solid line this ratio versus arc length for a late time. As can be seen, the ratio remains larger than 8. In the inner region the segment length was kept at eight times the distance of closest approach between nonlocal segments. Results were essentially unchanged when the segment length was halved. Different initial core thicknesses always resulted in the same core thickness distribution for the inner solution.

VI. ELLIPTICAL CORES

All the results presented in Sec. V have a two-length-scale desingularization which accounts for mild core deformation. This is a way of extending the validity of the filament model to core deformations in the case of mild interaction of nonlocal filaments. A more detailed presentation of this model and its application to the problem of antiparallel vortex collapse is found in Pelz [14]. We alluded to this modification in Sec. II, but have chosen to present it after the results in order to give the physical ramifications.

When spherical core functions were used, as given in Eq. (2.2), a steady local solution did not develop, and the solution was not singular. The reason is clear: the core thicknesses in the inner region gradually increased. (Their rate of decrease was not as high as the spatial scale.) They eventually caused a core overlap between filament pairs in the dipoles. The mutual induced velocity decreased, causing the dipolar position to be farther away from the origin. This led to a decrease in the axial strain rate, which then led to further decreases in the rate of core thickness thinning. Eventually, the solution evolved to six separate antiparallel collapse

problems as the dipoles became more isolated. Also, when core overlap occurs, the filament model breaks down.

From observations of the field simulations, the cores deform mildly as they interact with their dipolar twin (see, for example, Figs. 13 and 26 in Boratav and Pelz [3]). The cores elongate as they advect toward the symmetry plane which separates the antiparallel vortex tubes. The deformed cores will have a negligible effect on the nonlocal dynamics, but will effect the local intratube dynamics and possibly the dipolar dynamics.

The way this core deformation was accounted for in the filament model was through a two-length-scale core function, instead of the symmetric core function which has one length scale. For symmetric cores the local induced velocity is proportional to the local curvature (in the normal direction) and the core thickness, and directed in the binormal. For an elongated core, however, that part of the velocity coming from the curvature in the elongated direction should be proportional to a representative thickness in that direction. Likewise, that part of the velocity coming from the shortened direction should involve the smaller core thickness. The local induced velocity is then not necessarily in the binormal, but has rotated toward the elongated direction.

Although imprecise, we refer to this two-scale desingularization as the elliptical core model, where the semimajor axis is in the direction of elongation. Dynamic equations for the orientation and eccentricity could be written based on the strain field; however, we use a more *ad hoc* closure. For each segment, we find, in a plane transverse to the tangent, two orthonormal vectors. One is pointed toward the symmetry plane, and the other pointed parallel to it. They are the semiminor and semimajor axes, respectively. In the transverse plane, if the core thickness is greater than the distance to the symmetry plane, then the semiminor length is that latter distance. The semimajor length is then set to preserve the cross-sectional area.

This model will be valid only if the eccentricity is not too large. In the simulations, the largest eccentricity occurred at $s=0$, with the semimajor to semiminor ratio being 1.7. This ratio is plotted on the right-side axis in Fig. 13 (dashed). The ratio gradually decreases to 1 as the arc length increases.

The nonregularized Biot-Savart law was used for all nonlocal segment contributions to the induced velocity. This was justified due to the fact that the cores from nonlocal segments did not overlap with any nodes at which the velocity was evaluated. The difference between the regularized and nonregularized induced velocity from these nonlocal segments was negligible.

While there was no core overlap of nonlocal segments, the extent to which the centroid movement and point approximation to a elongated core is valid, however, must be checked. In particular, changes in the dipolar translation velocity from deformed cores may be significant. We shall try to provide bounds by using the exact two-dimensional (2D) solutions of translating dipoles with a constant vorticity distribution as found by Pierrehumbert [23] and Wu, Overman, and Zabusky [24].

In the 2D steady translating dipole solution with a normalized average radius of about 1.3 and an elongation of 1.7, the ratio of the actual induced velocity to that of a point vortex with the same circulation is about 0.85. Note that, since the shapes are not ellipses, the comparison is only approximate. Since our cubic Gaussian vorticity distribution is considerably more concentrated than the top hat distribution, this ratio is clearly a lower bound. A ratio much closer to 1 is expected, suggesting that the movement of the centroid and the use of the induced velocity of singular filament are valid approximations. Slight core flattening (but not too much) acting to reorient the local induction velocity seems to be necessary for the self-similar collapsing solution to occur.

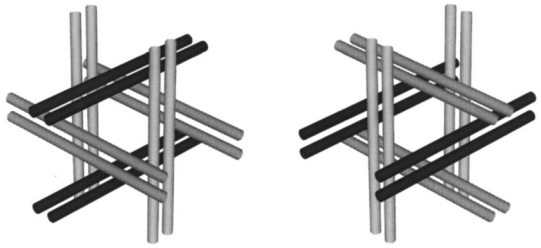

FIG. 14. Straight filament model of topology change before and after the critical time.

VII. AFTER THE CRITICAL TIME

In this section we speculate on the evolution of the flow after the critical time. From the pseudospectral Navier-Stokes simulations [3], the rapid collapse of the dodecapole, and coincident rise in peak vorticity, is followed by an equally rapid decrease in vorticity and an explosive ejection of small-scale vorticity from around the origin. Soon after, a nearly isotropic turbulent field develops.

Whereas it is difficult to ascertain the evolution of vortex-line topology during this time, an implosion (explosion) scenario is suggested. We therefore look for credible ''clean'' incoming (outgoing) states using the filament model, keeping in mind that the outgoing state is most likely unstable.

From examination of the filament configurations in Fig. 5, there are a number of possible topology changes which could occur. Simple dipolar reconnection may occur but, since the local induced velocity is still inward, a change subsequent to it must occur.

One particular state change which can occur through a series of reconnections is termed the ''pass-through'' scenario. The incoming and outgoing states are shown in the cartoon in Fig. 14. The black vortices which are moving toward the origin and straddle the vertical z axis, move away from their dipolar companions, pass through the dark gray and light gray vortices, pair with their images and move away from the origin straddling the y axis. The dark gray and light gray vortices behave similarly with permutation.

If the topology of the incoming state in Fig. 14 is unlinked, the outgoing topology is Brunnian linked as in Fig. 3(b), with an important exception—the circulation has changed sign (there is also a $\pi/2$ rotation). Since the sign reversal of circulation results in time-reversed dynamics, and since we have already established that the Brunnian-linked configuration collapses, the outgoing state is simply the time-reversed evolution of the Brunnian-linked configuration. There is, therefore, one local self-similar solution for $|t_{\rm crit}-t|\rightarrow 0$.

VIII. CONCLUDING REMARKS

We have identified a locally self-similar solution to a vortex filament model which has a pointwise singularity in real time. Put another way, we have established an attracting steady solution to the dynamically rescaled filament equations in which the logarithmic derivative of the scaling metric is a nonzero constant. Physically, six elongated vortex rings placed symmetrically about the origin, and straddling each axis, collapse toward the origin in such a way as to look steady in a frame whose magnification increases as $(t_{\rm crit}-t)^{-1/2}$ about the origin. It was necessary to model core deformation in order to attain this solution.

The scalings are as follows. The metric has the form $S=[2a(t_{\rm crit}-t)]^{-1/2}$. The position of point $\vec{x}_0$ of the fundamental filament is $\vec{x}_0=(1,4.6\ldots,0)[2a(t_{\rm crit}-t)]^{1/2}$. The velocity at $\vec{x}_0$ of the fundamental filament is $\vec{u}_0=-(1,4.6\ldots,0)[a/2(t_{\rm crit}-t)]^{1/2}$. The axial strain rate at the same point is $2a/(t_{\rm crit}-t)$. The average vorticity across the cross section at the same point is $\vec{\omega}_0=(0.59\ldots)(t_{\rm crit}-t)^{-1}$ where the constant $0.59\ldots$ is a function of the particular core shape.

The inner solution is attracting within a class of initial conditions with bilateral and permutation symmetries. Critical points within the collapsing structure suggest that fluid particles may be trapped there and singular focusing results. The sufficient condition for singularity of Ng and Bhattacharjee [21] has a particularly simple form in this model. It is conjectured that the topology change at the critical time allows a subsequent self-similar expanding solution with a change in the linkage of the vortex lines. It also suggests that the singularity is pointwise in time.

The $(t_{\rm crit}-t)^{-1}$ scaling of the vorticity and strain rate agrees with the theorems by Beale, Kato, and Majda [20] and Ponce [19]. The power of the length scale, $\frac{1}{2}$, obeys the seminorm estimate of $\frac{2}{5}$ or larger when velocity is not bounded (Constantin [25]). The theorem by Constantin and Fefferman [26] concerning the spatial correlation of the vorticity unit vector is not violated. Indeed, there are always orthogonal vortex lines in an $O(1)$ neighborhood of the rescaled frame, and there is nonzero curvature of the vortex lines.

Is there an Euler solution similar to that of the filament model? The extent to which core deformation occurs in the field solution and effects the subsequent dynamics is critical for determining the answer. It is encouraging that the well-known necessary conditions for consistency of filament solutions (large radius of curvature to core size, no core overlap) are satisfied. The visual similarity between isosurfaces of the field simulation in Fig. 1 and filament position in Fig. 5 is also supportive. To investigate whether there is a rate of strain present near the filaments which would cause severe deformation of material lines and hence vorticity contours, in Fig. 15 we plot a few streamlines at a late time in the rescaled frame in the plane $z=0$. The streamlines are elliptical reflecting the elliptical core distribution, but show little other deformation. Despite the divergence of the source flow being $3a$, the axial strain rate about the filaments creates a region with approximately closed streamlines.

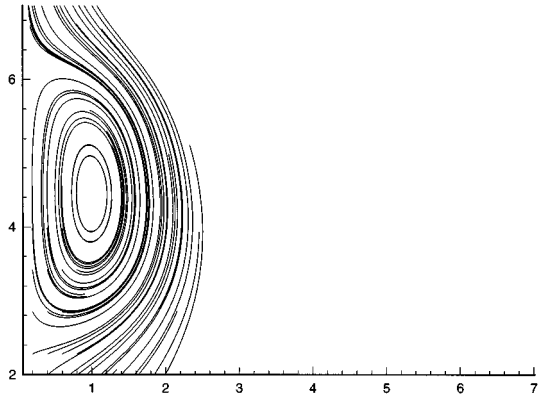

FIG. 15. Streamlines in the rescaled frame in the plane $z=0$ at a late time.

In summary, only a field simulation which displays a substantial scaling range and adequate resolution can determine whether there is a self-similar FTS to the incompressible Euler equations. The model solution in this paper provides a possible structure to the inner and outer solutions, scaling law predictions, and tools such as dynamic rescaling to carry out such simulations.

ACKNOWLEDGMENTS

Thanks go to A. Bhattacharjee, O. Boratav, W. Bottega, V. Fernandez, J. Greene, V. Malkin, D. Meiron, V. Scheffer, M. Shelley, E. Siggia, and N. Zabusky for useful discussions.

[1] C. R. Doering and J. D. Gibbon, *Applied Analysis of the Navier-Stokes Equations* (Cambridge University Press, Cambridge, 1995).
[2] R. M. Kerr, Phys. Fluids **5**, 1725 (1993).
[3] O. N. Boratav and R. B. Pelz, Phys. Fluids **6**, 2757 (1994).
[4] E. D. Siggia and A. Pumir, Phys. Rev. Lett. **55**, 1749 (1985).
[5] E. D. Siggia, Phys. Fluids **28**, 794 (1985).
[6] A. Pumir and E. D. Siggia, Phys. Fluids **30**, 1606 (1987).
[7] A. T. A. M. de Waele and R. G. K. M. Aarts, Phys. Rev. Lett. **69**, 2196 (1992).
[8] A. Pumir and E. D. Siggia, Phys. Fluids **2**, 220 (1990).
[9] M. J. Shelley, D. I. Meiron, and S. A. Orszag, J. Fluid Mech. **246**, 613 (1993).
[10] M. E. Brachet, M. Meneguzzi, A. Vincent, H. Politano, and P. L. Sulem, Phys. Fluids **4**, 2845 (1992).
[11] O. M. Knio and A. F. Ghoniem, J. Comput. Phys. **86**, 75 (1990).
[12] A. Leonard, Ann. Rev. Fluid Mech. **17**, 523 (1985).
[13] V. M. Fernandez, N. J. Zabusky, and V. M. Gryanik, J. Fluid Mech. **229**, 289 (1995).
[14] R. B. Pelz (unpublished).
[15] D. W. McLaughlin, G. Papanicolaou, C. Sulem, and P. L. Sulem, Phys. Rev. A **34**, 1200 (1986).
[16] B. J. LeMesurier, G. Papanicolaou, C. Sulem, and P. L. Sulem, Physica D **31**, 78 (1988).
[17] M. J. Landman, G. Papanicolaou, C. Sulem, P. L. Sulem, and

X. P. Wang, Physica D **47**, 393 (1991).
[18] W. J. Bottega, Quantum J. Mech. Appl. Math. **44**, 17 (1991).
[19] G. Ponce, Commun. Math. Phys. **98**, 349 (1985).
[20] J. T. Beale, T. Kato, and A. Majda, Commun. Math. Phys. **94**, 61 (1984).
[21] C. S. Ng and A. Bhattacharjee, Phys. Rev. E **54**, 1530 (1996).
[22] O. N. Boratav and R. B. Pelz, Phys. Fluids **7**, 1712 (1995).
[23] R. T. Pierrehumbert, J. Fluid Mech. **99**, 129 (1980).
[24] H. M. Wu, E. A. Overman II, and N. J. Zabusky, J. Comput. Phys. **53**, 42 (1984).
[25] P. Constantin, SIAM Rev. **36**, 73 (1994).
[26] P. Constantin and C. Fefferman, Indiana Univ. Math. J. **42**, 775 (1993).